GPS Solutions (2024) 28:63
https://doi.org/10.1007/s10291-023-01603-5

ORIGINAL ARTICLE

Estimation of phase center corrections for BDS satellites aligned to the IGS20 frame

Yongqiang Yuan[1] · Xingxing Li[1] · Yibin Yao[1] · Shi Huang[1] · Qingyun Wang[1] · Keke Zhang[1]

Received: 24 September 2023 / Accepted: 16 December 2023

Abstract

Precise information about the phase center corrections (PCCs) for BeiDou satellite antennas is not only essential to the generation of high-precision orbit and clock products but also important to the determination of terrestrial scale. However, the existing BDS PCCs still suffer from some deficiencies, such as the lack of phase center variations (PCVs) for several BDS satellites as well as the misalignment of phase center offsets (PCOs) and the latest IGS20 frame. We present the estimation results of both PCVs and PCOs for all 37 currently in-service BDS Inclined Geosynchronous Satellite Orbit (IGSO) and Medium Earth Orbit (MEO) satellites. The results demonstrate that the nadir-angle-dependent PCVs of the same satellite block type have fairly good consistency. The horizontal PCO estimates and the igs20.atx values have a consistency of several centimeters. As for the Z-PCOs aligned to IGS20 frame, the estimated values are 2380 and 530 mm smaller than the igs20.atx values for BDS-2 IGSO and BDS-2 MEO satellites, while those of BDS-3 MEOs have mean differences of −61 and 46 mm with respect to igs20.atx values for satellites manufactured by the China Academy of Space Technology and Shanghai Engineering Center for Microsatellites, respectively. By using the estimated PCCs instead of the igs20.atx values, the precise orbit and clock determination precision can be improved by 5–32% and 4–20%, respectively. Furthermore, applying the estimated PCCs, the scale factors determined by BDS solutions exhibit good consistency with IGS20 frame, with mean scale differences below 0.15 ppb.

Keywords Phase center variation · Phase center offset · BDS · Precise orbit determination · Terrestrial scale · Solar radiation pressure

Introduction

The phase center correction (PCC) of the satellite transmitting antenna is a crucial error source in high-precision Global Navigation Satellite System (GNSS) data processing. To describe the satellite antenna phase center corrections, the phase center offset (PCO) is defined as a vector from the satellite center of mass (CoM) to the mean phase center. In addition to PCO, the antenna phase center also changes with the signal direction, and the additional variation with respect to PCO is known as the phase center variation (PCV). To achieve high-precision GNSS solutions, both PCO and PCV must be precisely calibrated or modeled.

Based on a global ground network equipped with absolutely calibrated receiving antennas, the PCC can be estimated for the satellite transmitting antennas if the scale of the ground network is fixed to a known reference frame (Ge et al. 2005a). Extensive studies have been carried out following this approach for the estimation of GPS and GLONASS

✉ Xingxing Li
xxli@sgg.whu.edu.cn

Yongqiang Yuan
yqyuan@whu.edu.cn

Yibin Yao
ybyao@whu.edu.cn

Shi Huang
huangshi2016@whu.edu.cn

Qingyun Wang
qywang@whu.edu.cn

Keke Zhang
kkzhang@whu.edu.cn

[1] School of Geodesy and Geomatics, Wuhan University, 129 Luoyu Road, Wuhan 430079, Hubei, China

Published online: 20 January 2024

satellite phase center corrections (Schmid et al. 2007; Dilssner et al. 2010). Since the estimation of the vertical component of PCOs depends on the scale of a certain reference frame, such as the International Terrestrial Reference Frame (ITRF), once a new reference frame is used, the estimation should be re-performed to keep scale consistency. As a result, the International GNSS Service (IGS; Johnston et al. 2017) has provided several sets of satellite antenna PCCs in the Antenna Exchange Format, such as the igs08.atx, the igs14.atx, as well as the igs20.atx, which fixed their scale to ITRF2008, ITRF2014, and ITRF2020 solutions, respectively (Rebischung et al. 2012; Rebischung and Schmid 2016; Villiger 2022; Masoumi 2022).

In addition to GPS and GLONASS, new GNSS constellations have been developed in recent years, including Galileo of Europe and the BeiDou Navigation Satellite System (BDS) of China. The current BDS constellation consists of a total of 45 satellites, including 15 satellites from the regional BeiDou navigation satellite system (BDS-2) and 30 satellites from the global BeiDou navigation satellite system (BDS-3). Several studies have made efforts to estimate the PCCs for BDS-2 Inclined Geosynchronous Satellite Orbit (IGSO) and Medium Earth Orbit (MEO) satellites (Dilssner et al. 2014; Guo et al. 2016; Huang et al. 2018), but quite large discrepancies were found in the Z-component PCO estimations, which can even exceed 1 m for BDS-2 IGSO satellites. This could be attributed to the use of GPS L1/L2 phase center corrections for BDS signals in ground receiving antennas. More recently, Dilssner et al. (2020), Xia et al. (2020), and Qu et al. (2021) have estimated the B1I/B3I PCOs and PCVs for BDS-3 MEO satellites, but unfortunately, their PCC estimates are only available for satellites with satellite vehicle number (SVN) up to C219.

In CSNO (2019a), the China Satellite Navigation Office (CSNO) published the band-specific manufacturer phase center corrections for all BDS satellites. Nevertheless, several deficiencies were identified for these CSNO values. First, these CSNO values only include satellite PCOs, but no information about phase center variations is provided. At the same time, the calibration quality of CSNO PCOs exhibits disparities for individual spacecraft, and the CSNO PCOs of BDS-2 satellites are found to be in poor consistency with the IGS antenna model (Xia et al. 2020; Zajdel et al. 2022). Thus, it is important to generate consistent and accurate PCO and PCV estimates for all currently in-service BeiDou IGSO and MEO satellites.

Due to the strong correlation between satellite Z-component PCO and station height, the Z-component PCOs must be aligned to the scale of the specific terrestrial reference frame. On November 27, 2022 IGS switched its reference frame to the latest IGS20, and the corresponding satellite Z-component PCOs were adjusted for alignment for GPS, GLONASS, and Galileo. However, this is not the case for BDS. In current igs20.atx, the PCOs of BDS-3 are the CSNO values, while those of BDS-2 are mean values of the estimation results from different institutions. These could lead to inconsistency between BDS and GPS/GLONASS/Galileo solutions. Therefore, it is of great significance to estimate BDS satellite PCCs in the latest IGS20 frame, which is the main research objective of this study.

After this introduction, the datasets used in BDS PCC estimation are introduced, and the method and processing strategies of PCC estimation are summarized. Subsequently, the estimation results of nadir-angle-dependent PCVs and PCOs are demonstrated. After that, the estimated BDS PCCs are validated by their precise orbit, precise clock, and terrestrial scale determination performances, respectively. The summary and conclusion are given in the last section.

BDS constellation and tracking network

All the 15 satellites of the BDS-2 constellation were manufactured by the China Academy of Space Technology (CAST), including 5 Geostationary Earth Orbit (GEO), 7 IGSO, and 3 MEO satellites. Unlike BDS-2, the 30 BDS-3 satellites were developed by two different manufacturers. CAST manufactured the 3 GEOs, 3 IGSOs and 14 MEOs, while the remaining 10 MEO satellites were manufactured by the Shanghai Engineering Center for Microsatellites (SECM). In this study, we focus our attention on the 37 IGSO and MEO satellites, and the 8 GEO satellites are not included since it is difficult to estimate their PCCs with ground tracking data due to the poor observing geometry. In addition, historic satellites such as C014 as well as the BDS-3 experimental satellites, are not considered since they are out of service.

To obtain accurate estimations for BDS satellite PCOs and PCVs, the phase center of receiving antennas needs to be well calibrated. For this purpose, the multi-frequency robot calibrations provided by Geo++ (Schmitz et al. 2008; Villiger 2022) are used for the phase center correction of the receiving antennas. Since the dual-frequency IF combination of B1I and B3I is formed to eliminate the first-order ionospheric delay, only the antennas with B1 and B3 calibrations are considered. As a result, a total of 17 antenna types are selected for BDS PCC estimation, and their general information is summarized in Table 1. In the IGS multi-GNSS tracking network, more than 240 stations are equipped with these receiving antennas (as of December 2022). In this study, 149 stations with BDS B1I and B3I tracking ability are selected to estimate BDS PCCs, and the station distribution is shown in Fig. 1.

In order to have a better estimation of BDS satellite PCCs, the dataset of 2 years from day of year (DOY) 001, 2021 to DOY365, 2022 was processed. Figure 2 shows the

Table 1 Ground receiving antennas used in BDS satellite PCC estimation

Antenna	Radome	Antenna	Radome
JAVRINGANT_DM	NONE	SEPCHOKE_B3E6	SPKE
JAVRINGANT_DM	SCIS	TPSCR.G3	NONE
JAV_GRANT-G3T	NONE	TPSCR.G3	SCIS
LEIAR20	LEIM	TPSCR.G5	TPSH
LEIAR20	NONE	TRM115000.00	NONE
LEIAR25.R3	LEIT	TRM57971.00	NONE
LEIAR25.R3	NONE	TRM59800.00	NONE
LEIAR25.R4	LEIT	TRM59800.00	SCIS
LEIAR25.R4	NONE		

daily number of tracking stations for different BDS satellites. As can be seen, BDS-2 MEOs and BDS-3 MEOs with SVNs up to C212 are tracked by most ground stations, followed by BDS-3 MEOs with SVNs C213-C219, BDS-2 IGSOs, BDS-3 MEOs with SVNs C222-C228, and the three BDS-3 IGSOs. Although there were only about 20 stations tracking BDS-3 IGSOs in the beginning of 2021, the number increased to about 40 after DOY050, 2021, and even reached 70–80 in 2022. In general, for most days, the number of tracking stations is more than 60 and 40 for MEO and IGSO satellites, respectively, guaranteeing sufficient ground observation data for the PCC estimation.

Methodology of BDS PCC estimation

In this section, the methods of BDS satellite PCO and PCV estimation are presented. The modeling of solar radiation pressure for the BDS satellite is also described. At the same time, the data processing strategies are summarized.

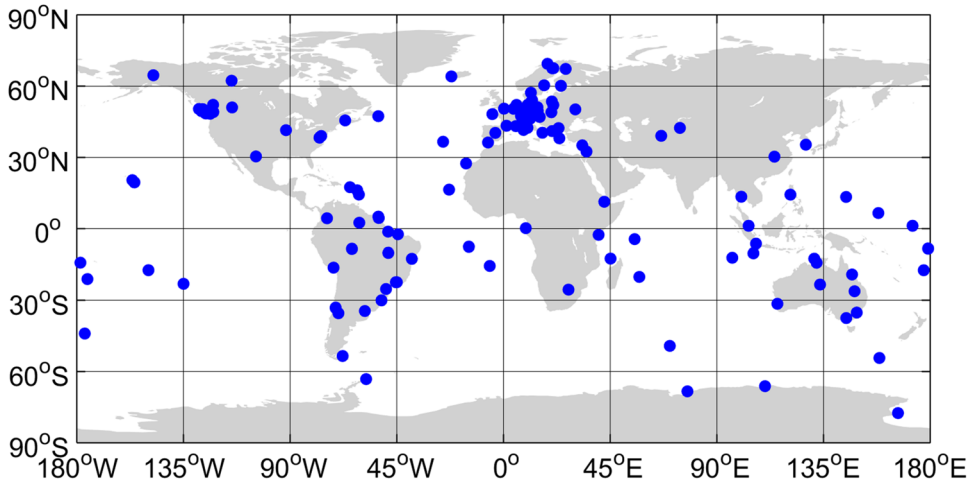

Fig. 1 Distribution of BDS tracking stations selected for PCC estimation

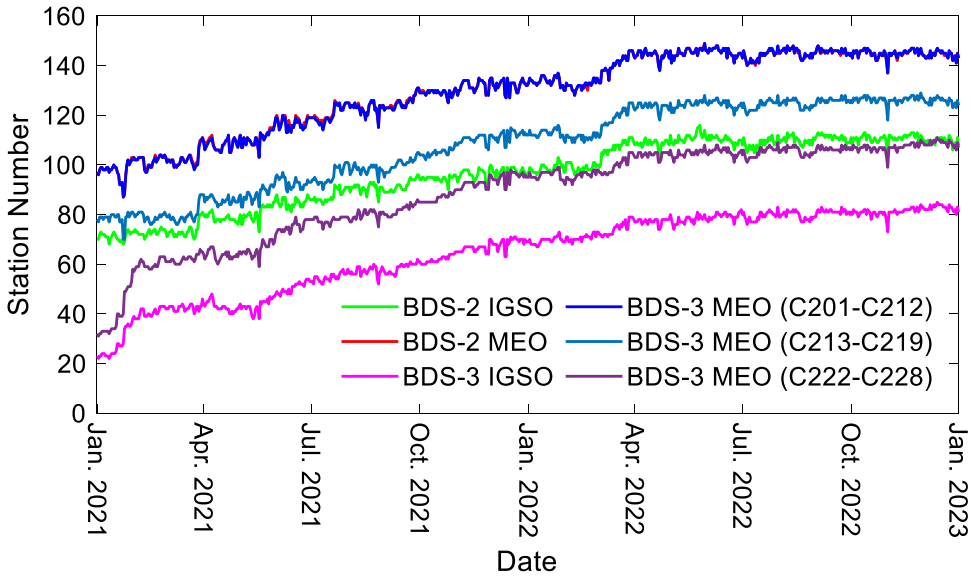

Fig. 2 Number of BDS tracking stations over DOY001, 2021 and DOY365, 2022

Table 2 Strategies of BDS phase center correction estimation

Items	Models
Basic observations	Undifferenced ionosphere-free code and carrier phase observations of B1I/B3I; 5 min sampling
Arc length	72 h
Cutoff elevation	7 degrees
Weighting	Elevation-dependent weighting: 1 for E > 30 deg, otherwise 2*sin(E)
Group delay variation	Corrected for BDS-2 satellites with the empirical correction model by Wanninger and Beer (2015)
Geopotential	Earth Gravitational Model 2008 (Pavlis et al. 2012) up to 12 × 12
Third body effects	Considering all planets using DE421 (Folker et al. 2009)
Solid earth tide, pole tide, and ocean tide	Their effects on geopotential and station displacement are considered with the models in IERS conventions 2010 (Petit and Luzum 2010); FES2014b (Carrere et al. 2016) is used for ocean tides
SRP models	9-parameter adjustable box-wing model
Earth albedo and infrared radiation forces	Considered with the model proposed by (Rodriguez-Solano et al. 2011); assumed values of 0.8, 0.1, and 0.1 are used as absorption, specular reflection, and diffuse reflection coefficient for infrared radiation
Antenna thrust	Considered with transmit power values of 185 W, 130 W, 310 W, and 280 W for BDS-2 IGSO, BDS-2 MEO, BDS-3 MEO CAST and BDS-3 IGSO, and BDS-3 MEO SECM satellites, respectively (Steigenberger et al. 2017; Guo et al. 2023)
Satellite attitude	Continuous yaw-steering modes for BDS-2 IGSO C005/C017/C019, BDS-2 MEO C015, BDS-3 IGSO, and BDS-3 MEO satellites (Dilssner 2017; Li et al. 2018); other BDS-2 satellites enter orbit-normal mode when the Sun's elevation above the orbital plane is less than about 4 degrees
Stochastic orbit parameters	Not considered
Phase center corrections of satellite transmitting antennas	In satellite PCVs estimation: the PCOs are fixed to the values by igs20.atx; the PCVs at each nadir angle are estimated together with zero-mean constraint over all nadir angles In satellite PCOs estimation: the PCVs are fixed to the estimated block-specific values; the X-, Y-, and Z-PCO corrections are estimated with 10, 0.1, and 10 m constraints
Phase center corrections of ground receiving antennas	Corrected with the antenna calibrations by igs20.atx
Station coordinates	Fixed to IGS20 coordinates for IGS20 stations; estimated for other stations
Tropospheric delay	Estimating zenith wet delays and gradients as piecewise constants in 2 h and 24 h intervals, respectively, after a priori correction by Saastamoinen model using Global Pressure and Temperature model (Boehm et al. 2007) as well as Global Mapping Function (Boehm et al. 2006)
Satellite and receiver clock offsets	Epoch-wisely estimated as white noise
Phase ambiguities	Double differenced ambiguities resolution (Ge et al. 2005b)

PCO and PCV estimation

The effect of the phase center corrections of both transmitting and receiving antennas on the observed distance can be expressed by

$$\tilde{\rho} = \left| \left(r^S + R_{scf2crs} \cdot PCO^S \right) - \left(r_R + R_{enu2crs} \cdot PCO_R \right) \right| + PCV^S(\eta) + PCV_R(\alpha, e) \quad (1)$$

where r^S and r_R are the position of the satellite center of mass and the receiver reference point in the inertial frame, respectively. PCO^S is the phase center offset vector of the satellite transmitting antenna expressed in the spacecraft-fixed frame, and $R_{scf2crs}$ is the rotation matrix from the spacecraft-fixed frame to the inertial frame. PCO_R is the phase center offset vector of the receiving antenna in the topocentric coordinate frame, and $R_{enu2crs}$ is the rotation matrix from the topocentric coordinate frame to the inertial frame. η is the nadir angle

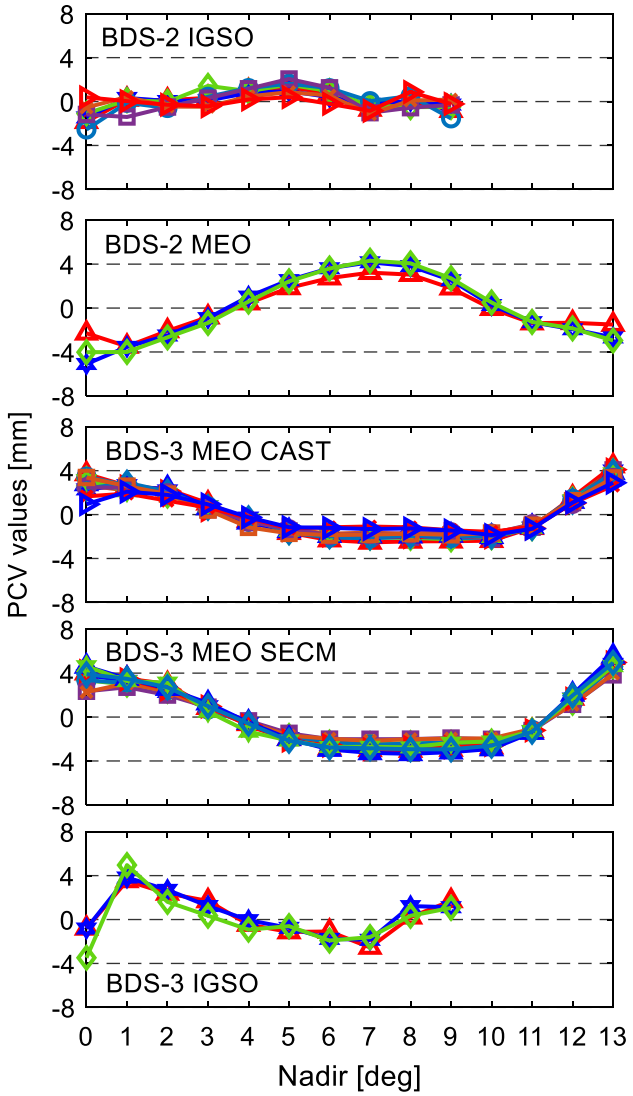

Fig. 3 Satellite-specific nadir-dependent B1I/B3I phase center variations of BDS satellites

seen from the satellite to the receiver; e and α are the elevation angle and the azimuth angle of the satellite with respect to the receiver, respectively. $PCV^S(\eta)$ is the nadir-dependent PCV of the satellite transmitting antenna, and $PCV_R(\alpha, e)$ is the elevation- and azimuth-dependent PCV of the receiving antenna.

The PCOs and PCVs of the receiving antennas are corrected with the multi-frequency calibrations, while those of the satellite transmitting antennas are estimated using ground tracking data. However, they cannot be estimated simultaneously due to the high correlation between PCOs and PCVs. Therefore, we estimate the PCOs and PCVs in two steps. First, we estimate the raw PCVs for each satellite where the PCOs are fixed to the values in igs20.atx. The nadir-dependent raw PCVs are modeled as a piecewise linear function with 1-degree resolution, and the initial value at each nadir angle is set to 0. The maximum nadir angles are set to 9 degrees and 13 degrees for BDS IGSO and MEO satellites, respectively. Although the maximum nadir angle of about 13.2 degrees can be reached for BDS MEO satellites, it is difficult to expand BDS MEO PCV pattern to 0–14 degrees due to the limited number of ground observations for nadir angles larger than 13 degrees. In order to prevent the normal equation system from becoming singular, a constraint is added to the normal equation, namely, that the sum of raw PCVs at all nadir angles equals zero (Schmid et al. 2007). Since PCVs are highly correlated with Z-PCO, the raw PCVs could be contaminated or biased. Therefore, a separate adjustment model is established to extract PCVs from the raw PCV estimates:

$$\sum_{i=0}^{n} \left[PCV^S_{raw}(\eta_i) - a - \Delta Z \cdot \left(1 - \cos \eta_i\right) \right]^2 = \min \tag{2}$$

where a is a constant parameter, and n is the number of PCV parameters. ΔZ is the Z-offset correction absorbed into the raw PCVs. The residuals of this least square adjustment are PCV estimates. This model has also been used for GPS and GLONASS PCV estimation (Schmid et al. 2007, 2016).

After obtaining the PCV estimates, the PCO corrections with respect to igs20.atx values are estimated. Considering the high correlation between Z-PCOs and the scale of the terrestrial reference frame, the coordinates of the IGS20 stations are fixed to IGS20 values to align the estimated Z-PCOs to the IGS20 scale. The tri-dimensional IGS20 coordinates can be calculated by using the coordinates and velocities at the reference epoch (2015.0) as well as the post-seismic deformation corrections (Altamimi et al. 2023). The seasonal terms are not considered since they are not implemented by IGS for the time being. Furthermore, to reduce the correlation between horizontal PCOs and orbital parameters as well as the correlation between vertical PCOs and satellite clock offsets, different constraints of 10 m, 0.1 m, and 10 m are added to X-, Y-, and Z-PCO parameters, respectively.

As the main non-conservative orbit perturbation, the modeling of solar radiation pressure (SRP) has an obvious impact on PCO estimation. The SRP can be modeled in both empirical and analytical ways. It has been demonstrated that with accurate satellite geometry and optical properties, the

Table 3 Final B1I/B3I PCV estimates for BDS-2 and BDS-3 IGSO/MEO satellites (unit: mm)

Nadir [deg]	BDS-2 IGSO	BDS-3 IGSO	BDS-2 MEO	BDS-3 MEO CAST	BDS-3 MEO SECM
0	−1.18	−1.70	−3.80	2.73	3.64
1	−0.06	4.10	−3.68	2.44	3.24
2	−0.24	2.23	−2.42	1.96	2.55
3	0.24	1.09	−1.03	0.64	0.88
4	0.82	−0.48	0.70	−0.56	−0.64
5	1.25	−0.83	2.27	−1.47	−1.90
6	0.70	−1.59	3.32	−1.83	−2.50
7	−0.61	−2.00	3.90	−1.89	−2.65
8	0.09	0.59	3.65	−1.86	−2.64
9	−0.50	1.30	2.35	−1.88	−2.54
10	–	–	0.24	−1.98	−2.41
11	–	–	−1.31	−1.14	−1.25
12	–	–	−1.71	1.20	1.56
13	–	–	−2.38	3.68	4.73

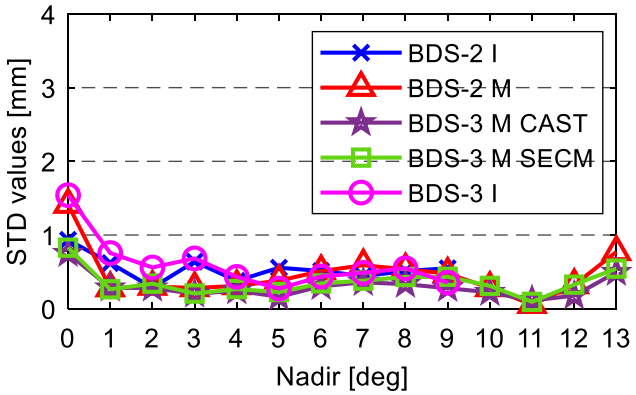

Fig. 4 Standard deviation values of satellite PCVs for different block-types

hybrid SRP model combining both empirical and analytical ones, such as the a priori box-wing model, can improve the precise orbit determination performances of GNSS satellites (Bury et al. 2019; Li et al. 2019, 2020). According to Fliegel et al. (1992), the SRP accelerations generated by the solar panel and the satellite bus can be formulated as follows:

$$a_{SP} = -\frac{A_{SP}}{M}\frac{S_0}{c}\frac{1AU^2}{r_S^2}\cos\theta_{SP}\left[(\alpha_{SP}+\delta_{SP})\vec{e}_D + 2\left(\frac{\delta_{SP}}{3}+\rho_{SP}\cos\theta_{SP}\right)\vec{e}_{N,SP}\right] \tag{3}$$

$$a_i = -\frac{A_i}{M}\frac{S_0}{c}\frac{1AU^2}{r_S^2}\cos\theta_i\left[(\alpha_i+\delta_i)\left(\vec{e}_D+\frac{2}{3}\vec{e}_{N,i}\right) + 2\rho_i\cos\theta_i\vec{e}_{N,i}\right] \tag{4}$$

where M is the mass of the satellite, A_{SP} and A_i are the area of the solar panel and the satellite's body surfaces. α_{SP}, ρ_{SP}, and δ_{SP} are the absorption coefficient, specular reflection coefficient, and diffuse reflection coefficient of the solar panel; α_i, ρ_i, and δ_i are coefficients for the surfaces of the satellite bus. S_0 is the solar flux at 1 astronomical unit (AU), c is the speed of light in vacuum. r_S is the instantaneous distance between the satellite and the sun, and $1AU^2/r_S^2$ is the scaling factor for the solar flux. θ_{SP}/θ_i is the angle enclosed by the unit vectors $\vec{e}_D$ (pointing from the satellite to the sun) and $\vec{e}_{N,SP}/\vec{e}_{N,i}$ (normal to the solar panel or the surface of satellite bus).

The box-wing model depends on proper knowledge of the geometry and optical properties of the satellite. However, only the absorption coefficients were released for BDS satellite optical properties, while the specular and diffuse reflection coefficients are still unknown (CSNO 2019b). In that case, the adjustable box-wing model (ABW) proposed by Rodriguez-Solano et al. (2012) is used. There are 9 parameters to be estimated in the ABW model, including the solar panel scaling factor, the absorption plus diffuse reflection coefficients of +X/+Z/–Z surfaces, the specular reflection coefficients of +X/+Z/–Z surfaces, the solar panel's rotation lag, and the so-called Y-bias. The initial values of the solar panel scaling factor and the optical coefficients of satellite bus are set to published values (with assumed coefficients for the specular and diffuse reflection, like Li et al. 2019 and Zhao et al. 2022), and the initial values of the rotation lag as well as Y-bias are set to zero. The PCO and ABW parameters are estimated simultaneously, and an iterative processing strategy is applied to further enhance the strength of solutions. The loose constraint of 0.3 is initially added to the ABW parameters, and after two iterations, the constraints are changed to tighter values of 0.001 and 0.01 for the solar panel scaling factor and other parameters, respectively. In the subsequent iteration, the simple mean of the PCOs obtained from the previous iteration is used as initial

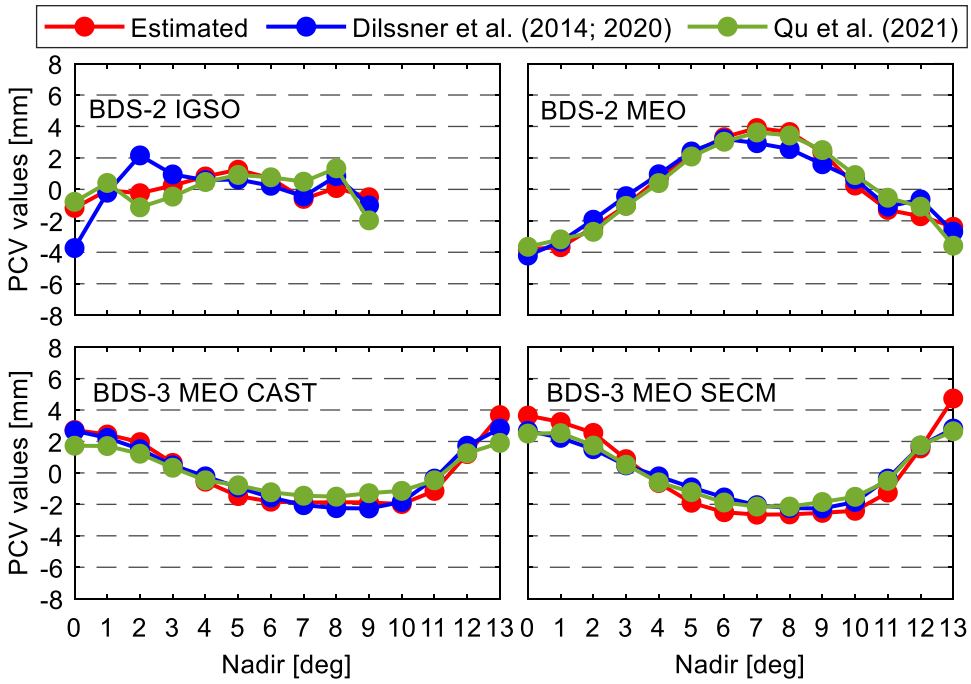

Fig. 5 Comparison of the estimated B1I/B3I PCVs with the values by Dilssner et al. (2014, 2020) and Qu et al. (2021)

value of this iteration, while the constraints on PCO parameters remain unchanged. Please note that the ABW parameters are solved in each 3-day solution. Solving long-term ABW parameters by stacking all the normal equations would be an alternative approach to improve the PCO estimation. For more information about the ABW model, one may refer to Rodriguez-Solano et al. (2012) and Duan et al. (2019).

Processing strategies

The ground BDS tracking data of 2 years are processed by a modified version of the GNSS + REsearch, Application and Teaching (GREAT) software developed by the School of Geodesy and Geomatics, Wuhan University (Li et al. 2021). The processing arc length is set to 72 h with 5 min sampling. Ionosphere-free code and carrier phase combinations are used to eliminate the first-order ionospheric delays, and the weights of observations depend on elevation. Other detailed information about the observation selection, the dynamical modeling, and the estimated parameters are summarized in Table 2.

BDS PCC estimation results

This section first investigates the PCV estimates of different block types, and then presents the PCO estimation results in the IGS20 frame. At the same time, PCVs and PCOs are compared with the values estimated by other institutions to further verify their credibility.

Phase center variations

Figure 3 shows the estimated PCV values as the function of the nadir angle for each IGSO and MEO satellite. These values are derived from all the 730 PCV solutions through unweighted averaging. To avoid possible errors brought by mismodeling of satellite attitude, the PCV estimates during eclipse periods are not considered. The PCV estimates of BDS-3 IGSOs are only based on the results of 2022 since the stations tracking BDS-3 IGSO satellites are only about 20–40 in the beginning of 2021. As can be found, for BDS-2 IGSO, BDS-2 MEO, BDS-3 MEO CAST, and BDS-3 MEO SECM satellites, the individual PCV estimates of the same block type exhibit quite good repeatability. At most nadir angles, the satellite-to-satellite PCV differences are less than 2 mm. The PCV values of BDS-3 MEO satellites show a significant nadir-dependent characteristic with variations ranging from −3.3 to + 5.5 mm, whereas the results of BDS-2 MEO exhibit the opposite pattern ranging from −5.1 to + 4.3 mm. As for IGSO satellites, the BDS-2 PCV values range from −2.5 to + 2.1 mm, while those of BDS-3 IGSOs vary from −3.5 to + 5.0 mm.

Considering the good consistency between individual PCV estimates of the same block type, the individual PCVs of the same block type are then simply averaged to generate the final block-mean PCV estimates (Table 3). The standard deviation (STD) values of different satellite PCVs are used as indicators to measure the quality of final PCV estimates, as shown in Fig. 4. It is clear that the PCV values of satellites in the same block type have good consistency, with the STD values around 0.5 mm in the majority of nadir-angles.

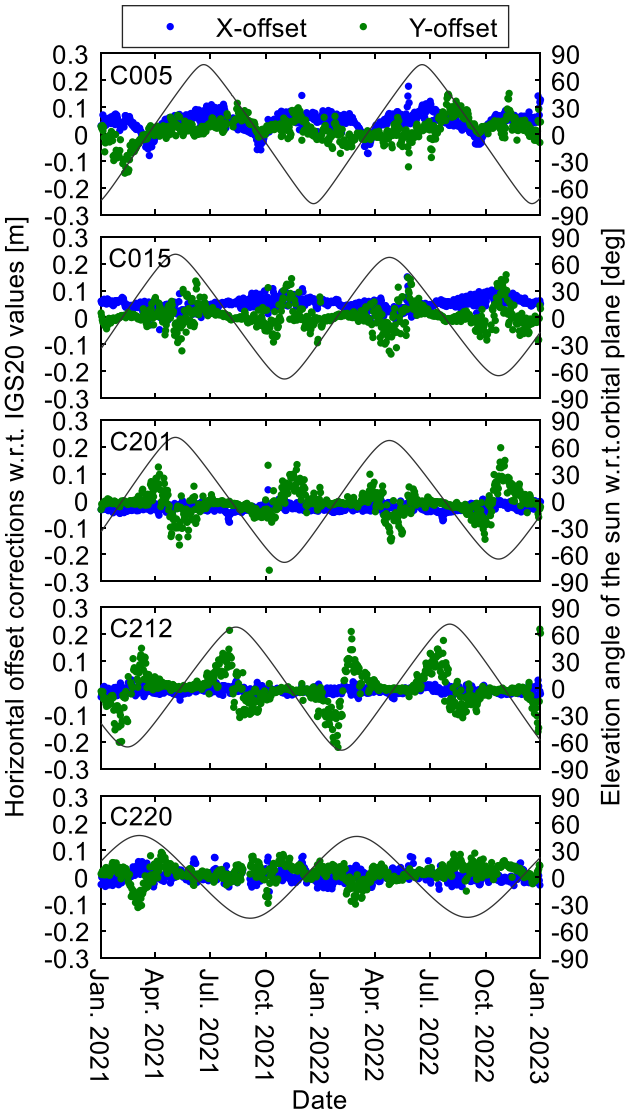

Fig. 6 Estimated X-offset and Y-offset corrections with respect to igs20.atx values for C005, C015, C201, C212, and C220

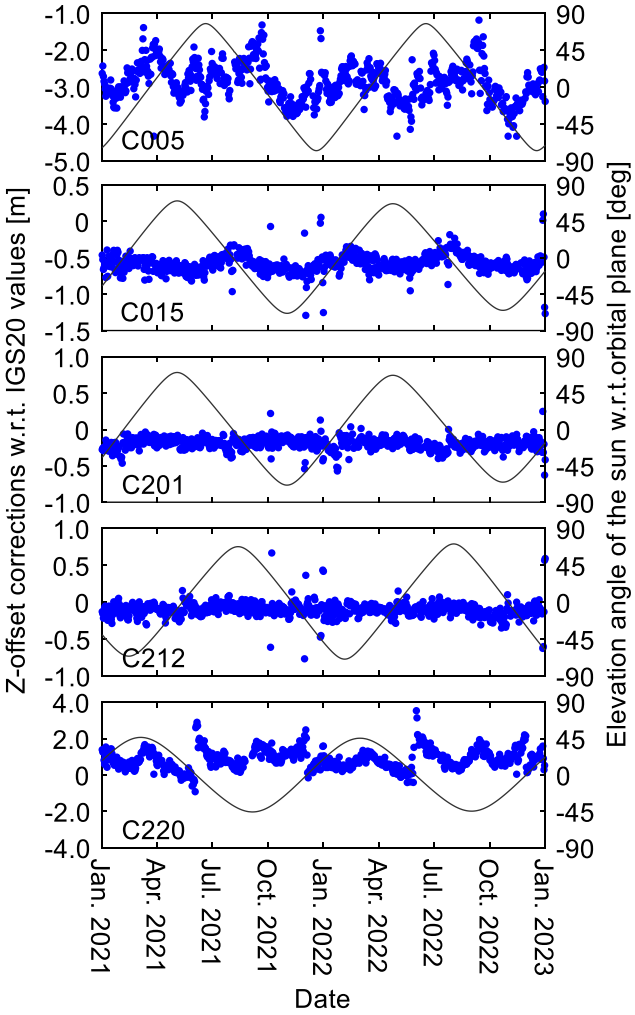

Fig. 7 Estimated Z-offset corrections with respect to igs20.atx values for C005, C015, C201, C212, and C220

Noteworthy, the STD values at 0 deg and the maximum nadir angle appear to be much larger than those at other angles, which is mainly due to the few observations at 0 deg nadir angle and the reduced weight of the observation at the maximum nadir angle. The IGSO solutions are worse than MEO solutions, mainly because MEO and IGSO satellites have different maximum ground observable nadir angles. The smaller range of nadir angle gives rise to a stronger correlation between the PCV parameter and other parameters, leading to a degradation in the PCV estimating quality for IGSO satellites.

To further verify the PCV estimates, Fig. 5 compares the estimated PCVs to the values by Dilssner et al. (2014, 2020) and Qu et al. (2021). In general, different sets of PCVs have similar shapes and magnitudes, and the PCV differences are within 1 mm at most nadir angles. Taking the root mean square (RMS) value of the PCV differences at all nadir angles as the indicator, the inconsistency between the estimated PCVs and those by Dilssner et al. (2014, 2020) and Qu et al. (2021) are (1.2, 0.8) mm, (0.6, 0.5) mm, (0.4, 0.7) mm, and (0.8, 0.8) mm for BDS-2 IGSO, BDS-2 MEO,

Table 4 Final B1I/B3I PCO estimates for BDS IGSO and MEO satellites (unit: mm)

Block Type	SVN	X-PCO	Y-PCO	Z-PCO	SVN	X-PCO	Y-PCO	Z-PCO
BDS-2 IGSO	C005	604.4	−3.6	2048.6	C010	611.9	−2.8	3232.2
	C007	621.5	−0.4	2488.7	C017	628.2	11.1	2133.2
	C008	611.8	5.9	2894.1	C019	649.1	−12.6	2086.0
	C009	613.2	−19.3	2877.2	–	–	–	–
BDS-2 MEO	C012	597.6	−1.8	1886.6	C015	609.4	3.4	1883.1
	C013	601.7	−1.7	2040.4	–	–	–	–
BDS-3 MEO CAST	C201	−232.8	−18.6	1826.8	C214	−198.7	−16.2	1950.9
	C202	−223.6	−18.7	1904.1	C218	−198.0	−13.3	1737.0
	C205	−225.7	−24.7	1903.3	C219	−199.0	−10.5	1740.9
	C206	−210.9	−9.7	1877.8	C222	−196.1	−12.1	1972.6
	C209	−209.0	0.5	1926.0	C223	−204.9	−12.3	1969.7
	C210	−204.5	−4.7	1970.9	C227	−199.7	−15.9	1837.4
	C213	−190.2	−11.1	1928.5	C228	−215.7	−16.0	1811.5
BDS-3 MEO SECM	C203	37.6	−3.0	1232.0	C212	63.5	−7.9	1005.9
	C204	36.0	1.6	1233.5	C215	64.4	−13.3	932.4
	C207	36.6	−12.0	1334.9	C216	67.7	−12.9	1099.8
	C208	32.6	−4.6	1281.9	C225	55.2	−11.1	1129.7
	C211	61.8	−10.7	1110.7	C226	71.6	−10.4	1204.2
BDS-3 IGSO	C220	−70.0	−296.3	3421.2	C224	−63.7	−293.4	3697.1
	C221	−85.4	−306.5	3383.8	–	–	–	–

BDS-3 MEO CAST, and BDS-3 MEO SECM satellites, respectively. These results indicate that the PCVs estimated in this study are of good quality.

Phase center offsets

After obtaining the PCV estimates, the PCOs are then estimated by fixing the IGS20 scale. Figure 6 shows the X- and Y-offset corrections with respect to igs20.atx values for representative satellites, i.e., C005 for BDS-2 IGSO, C015 for BDS-2 MEO, C201 for BDS-3 MEO CAST, C212 for BDS-3 MEO SECM, and C220 for BDS-3 IGSO. It can be seen that the variation of the Y-offset is related to the β -angle, and larger scatters are always accompanied by the larger absolute values of the β-angle. Peak-to-peak variations of about 0.3–0.4 m can be observed for periods with large absolute values of β-angle. As for the X-offset, the β -angle-dependency is less pronounced for MEO satellites. This could be attributed to the adoption of ABW which is a semi-analytical model rather than a purely empirical model with SRP parameters freely estimated. Previous studies have demonstrated that the X-PCO would be strongly correlated with SRP parameters when purely empirical SRP models such as ECOM and ECOM2 are used (Xia et al. 2020). Although optical coefficients are also estimated in ABW model, an appropriate constraint on these coefficients helps to decorrelate the SRP parameters and X-PCOs. Figure 7 shows the Z-offset correction series for C005, C015, C201, C212, and C220. Compared to the X- and Y-component, the Z-offset corrections are more scattered. The peak-to-peak variations are about 0.3–0.5 m for MEO satellites, while for IGSO satellites the peak-to-peak variations even exceed 2 m. The scatters of IGSO satellites are more dispersed than MEO satellites, which is mainly due to the smaller maximum nadir angle of IGSO satellites, making it more difficult to separate the Z-PCO from other parameters such as the satellite clock offset.

The final PCO estimates are then derived from the 730 three-day PCO series by unweighted averaging with a two-sigma criterion to detect and exclude the outliers in an iterative procedure. Table 4 lists the final B1I/B3I PCO estimates for all BDS IGSO and MEO satellites. The final X-PCO estimates of BDS-2 satellites are mainly within 598–628 mm except for C16, and the final BDS-2 Y-PCO estimates range from −20 to 11 mm. For BDS-3 MEO satellites, the two block types of CAST and SECM exhibit different X-PCO estimates, i.e., −233 to −190 mm for CAST and 32 to 72 mm for SECM, while the Y-PCOs of both types are around 0,

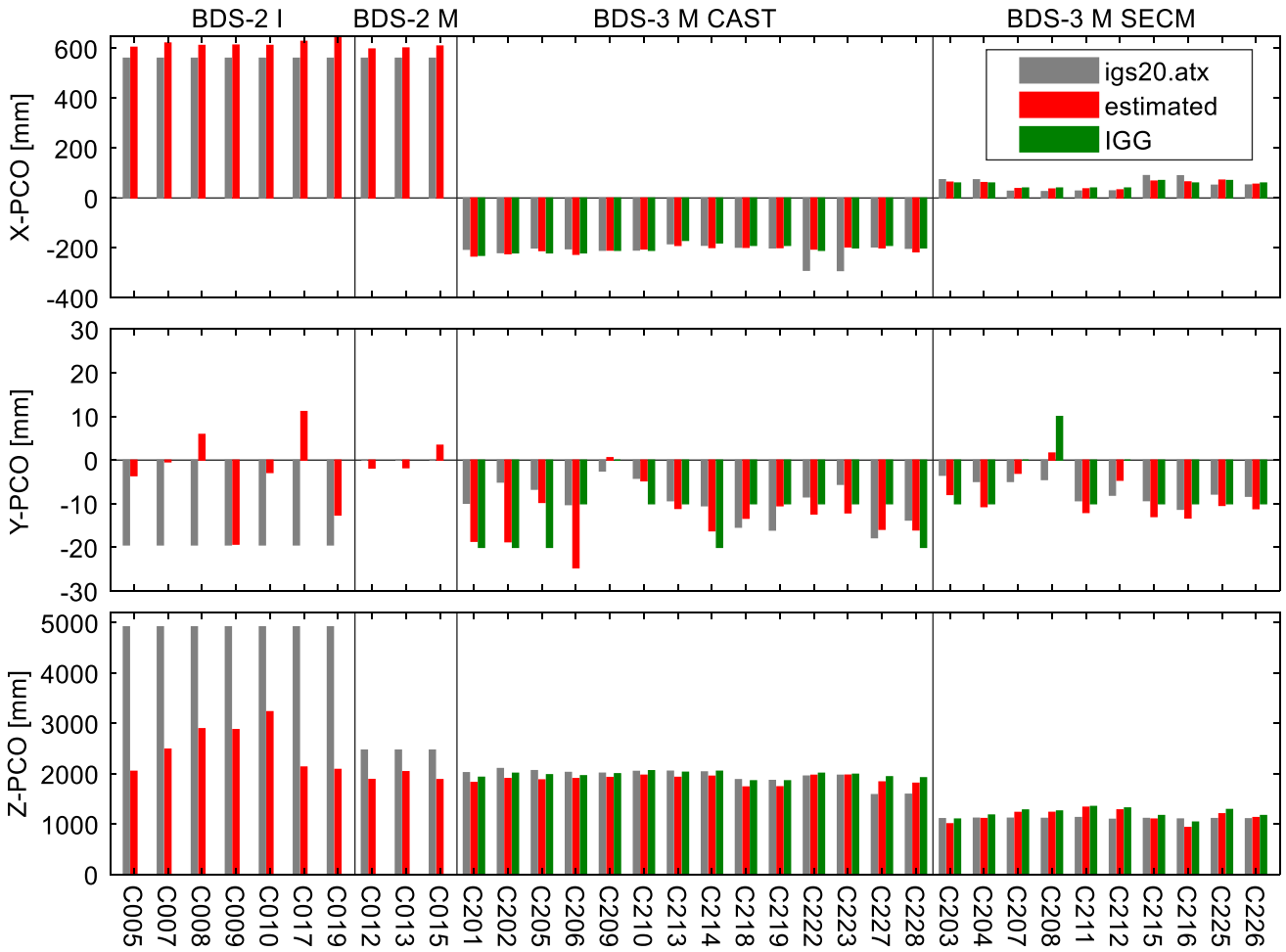

Fig. 8 Comparison of the estimated B1I/B3I PCOs with the values of igs20.atx and values by IGG

ranging from −25 to 2 mm. As for BDS-3 IGSO satellites, their X- and Y-PCO estimates are about −85 to −64 mm and −307 to −293 mm. The final Z-PCO estimates show large differences among satellites, ranging from 2049 to 3232 mm, 1883 to 2040 mm, 1737 to 1973 mm, 932 to 1335 mm, and 3384 to 3697 mm for BDS-2 IGSO, BDS-2 MEO, BDS-3 MEO CAST, BDS-3 SECM, and BDS-3 IGSO satellites, respectively.

Figure 8 further compares the PCO estimates with the values in igs20.atx (denoted as "igs20.atx") as well as those estimated by Zajdel et al. (2022; denoted as "IGG"). The IGSO satellites of BDS-3 are not displayed since the magnitude of their Y-PCOs is more than ten times that of other satellites. When compared to values in igs20.atx, the X-PCO estimates are on average 54 mm larger for BDS-2 IGSO and MEO satellites, while the mean difference of BDS-2 Y-PCO estimates with respect to igs20.atx values are 11 mm. For BDS-2 Z-PCOs, the estimated values are, on average, 2380 mm and 530 mm smaller than igs20.atx values for IGSO and MEO satellites, respectively. For BDS-3 MEO satellite, the final X-PCO estimates show differences ranging from −27 to 20 mm with respect to igs20.atx values, except for C222 and C223. The differences of the final Y-PCO estimates with respect to igs20.atx values are within −15 to 6 mm, with mean value of −3 mm. The Z-PCO estimates show larger variations from satellite to satellite, and the differences with respect to igs20.atx values are from −200 to 253 mm. For BDS-3 MEO CAST, the estimated Z-PCOs are smaller than the igs20.atx values, except for newly launched satellites of C225-C228. The average offset with respect to igs20.atx values is −134 mm when the four newly launched satellites are not considered but only −61 mm when all 14 satellites are considered. For BDS-3 MEO SECM, the estimated values are on average 46 mm larger than the igs20.atx values, while the differences of each satellite can be positive or negative.

When comparing the PCO estimates to the values reported by Zajdel et al. (2022), we can find that these two sets of PCOs have good consistency in the horizontal components, with mean differences of 3 and 2 mm for X- and

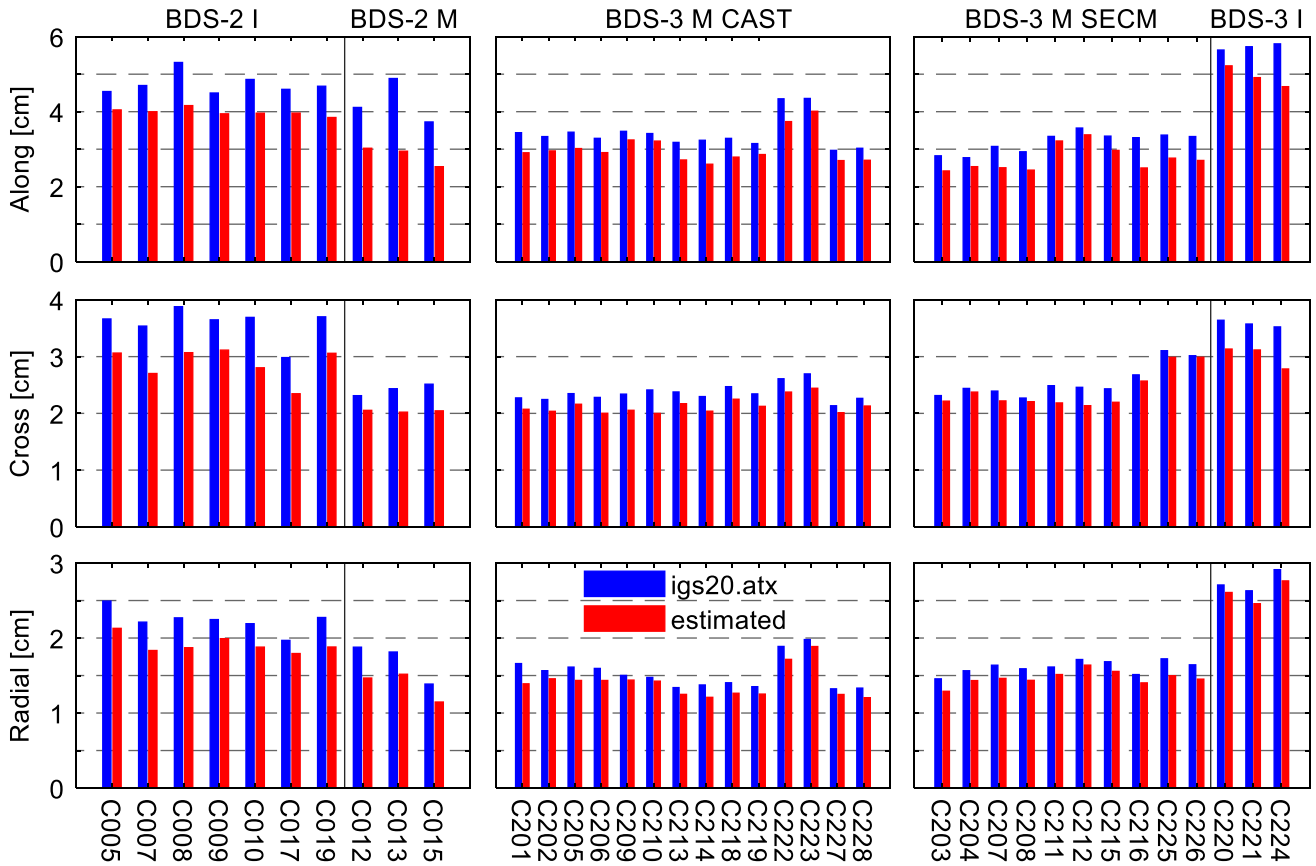

Fig. 9 24-h orbit overlapping RMS values of BDS satellites with different phase center corrections

Y-PCOs, respectively. As for the Z-PCO, the values estimated in this study are on average 77 mm smaller than those of Zajdel et al. (2022). Please note that the Z-PCOs by Zajdel et al. (2022) are aligned to IGS14 frame. The Z-PCO differences can be attributed to the scale differences between IGS20 and IGS14 as well as to the different software packages used.

Validation of the estimated BDS PCC

We then validate the estimated phase center corrections through precise orbit/clock determination and terrestrial scale determination. In the processing, the station coordinates are simultaneously estimated with satellite orbit and clock parameters, and the loose constraint of 1 m is used for each coordinate component. The minimum constraints of no-net-translation and no-net-rotation with respect to IGS20 frame are imposed on IGS20 stations.

The 24-h overlapping differences between two adjacent three-day solutions are used to validate the orbit and clock determination results. Figure 9 compares the average RMS values of 24-h orbit overlapping differences with different PCC values. It can be seen from the figure that all BDS satellites benefit from the estimated PCCs. Compared to the results with igs20.atx values, the average improvements in along-track, cross-track, and radial components are (15.7, 19.8, 14.4)% and (32.7, 15.6, 18.5)% for BDS-2 IGSO and MEO satellites, respectively, while smaller improvements of (11.8, 9.7, 8.4)%, (14.0, 6.1, 9.0)%, and (13.8, 15.9, 5.1)% are observed for BDS-3 MEO CAST, BDS-3 MEO SECM, and BDS-3 IGSO satellites. The orbit quality of BDS-2 satellites benefits more from the estimated phase center corrections than BDS-3 satellites, implying larger discrepancies between the actual phase center and igs20.atx values for BDS-2 satellites. Similarly, the STD values of 24-h clock overlapping are shown in Fig. 10. As can be found, the estimated PCCs decrease the STD values by 4–20% for all BDS satellites.

In addition to the orbit and clock determination performances, the performance of the estimated PCCs in terrestrial scale determination is also investigated. Two cases are studied, one with all BDS-2 and BDS-3 satellites, while the other with only BDS-3 satellites. The derived scale factors of BDS solutions with respect to the IGS20 frame is shown in Fig. 11. When both BDS-2 and BDS-3 satellites

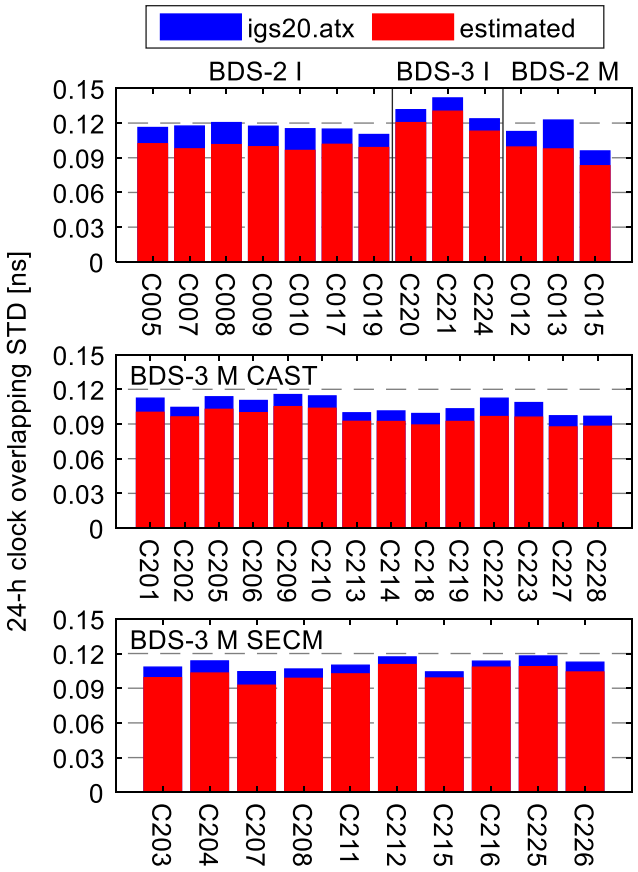

Fig. 10 STD values of 24-h clock overlapping comparison of BDS satellites with different phase center corrections

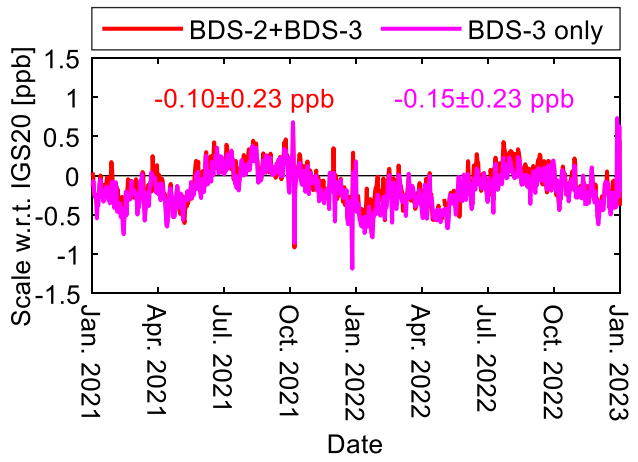

Fig. 11 Terrestrial scale with respect to IGS20 frame determined by BDS solutions

are included, the mean scale factor with respect to the IGS20 frame is −0.10 parts per billion (ppb), and the mean scale factor of BDS-3 only solutions is −0.15 ppb. These results indicate that the estimated PCCs are well aligned to the IGS20 frame.

Conclusions

This study presents the PCO and PCV estimation results for all BDS IGSO and MEO satellites. The nadir-angle-dependent PCVs are estimated as a piecewise linear function with 1-degree resolution. The results demonstrate quite good agreement among individual PCV estimates from the same block type, and the STD values of different satellite PCVs are smaller than 1 mm for most nadir angles. Therefore, the block-mean values over all satellites from the same type are derived as the final PCV estimates. The final PCV estimates are then compared with the values estimated by other researchers, and the results demonstrated good consistency among different sets of PCVs.

As for satellite PCO estimation, different characteristics can be identified for the PCO series of different components. The Y-PCO series shows significant dependency on β-angle, and the peak-to-peak variations reach 0.3 to 0.4 m during periods with large absolute values of β-angle. This β-angle-dependency is less pronounced for the X-PCO of MEO satellites due to appropriate constraints on SRP parameters. Compared to X- and Y-PCOs, the Z-offset series are more scattered, especially for IGSO satellites. The final PCO estimates are then derived and assessed. The final horizontal PCO estimates and the igs20.atx values have a consistency of several centimeters, while the final Z-PCO estimates exhibits 2380 and 530 mm smaller values on average for BDS-2 IGSO and BDS-2 MEO satellites. In addition, the mean differences of the final Z-PCO estimates with respect to igs20.atx values are −61 mm and 46 mm, for BDS-3 MEO CAST and BDS-3 MEO SECM satellites, respectively.

The estimated PCCs are then evaluated by their performances in precise orbit determination, precise clock estimation, and terrestrial scale determination. The results show that the orbit precision of all three components of along-track, cross-track, and radial benefits from the estimated PCCs, with improvements of 5–32% over the igs20.atx values. At the same time, the satellite clock precision can also be improved by 4–20%. Furthermore, the scale factors determined by BDS present mean values of −0.10 and −0.15 ppb with respect to the IGS20 frame for BDS-2 + BDS-3 and BDS-3 only solutions, respectively, which evidences the effective alignment of the estimated PCCs to IGS20 frame.

Supplementary Information The online version contains supplementary material available at https://doi.org/10.1007/s10291-023-01603-5.

Acknowledgements The International GNSS Service (IGS) is greatly acknowledged for providing multi-GNSS observation data. This study

is funded by the National Natural Science Foundation of China (Grant No. 42304019), China Postdoctoral Science Foundation (Grant No. 2023M732687), and the Open Fund of Hubei Luojia Laboratory (Grant No. 230100008). The numerical calculations in this paper have been done on the supercomputing system in the Supercomputing Center of Wuhan University.

Author Contributions Yongqiang Yuan and Xingxing Li designed the study and performed the research. All authors analyzed the data and were involved in writing the manuscript.

Data Availability The GNSS observation data can be downloaded from the IGS repository, https://cddis.nasa.gov/archive/gnss/data/. The IGS20 ANTEX file is available at https://files.igs.org/pub/station/general/igs20.atx. The BeiDou metadata can be found at http://en.beidou.gov.cn/SYSTEMS/Officialdocument/201912/P020200323536298695483.zip.

Declarations

Competing interests The authors declare no competing interests.

References

Altamimi Z, Rebischung P, Collilieux X, Métivier L, Chanard K (2023) ITRF2020: an augmented reference frame refining the modeling of nonlinear station motions. J Geod 97(5):47. https://doi.org/10.1007/s00190-023-01738-w

Boehm J, Niell A, Tregoning P, Schuh H (2006) Global Mapping Function (GMF): a new empirical mapping function based on numerical weather model data. Geophys Res Lett 33(7):L07304. https://doi.org/10.1029/2005GL025546

Boehm J, Heinkelmann R, Schuh H (2007) Short note: a global model of pressure and temperature for geodetic applications. J Geod 81(10):679–683. https://doi.org/10.1007/s00190-007-0135-3

Bury G, Zajdel R, Sośnica K (2019) Accounting for perturbing forces acting on Galileo using a box-wing model. GPS Solut 23(3):74. https://doi.org/10.1007/s10291-019-0860-0

Carrere L, Lyard F, Cancet M, Guillot A, Picot N (2016) FES 2014, a new tidal model—validation results and perspectives for improvements. In: ESA living planet conference, Prague 2016

CSNO (2019a) Satellite antenna phase center of BDS. China Satellite Navigation Office, http://en.beidou.gov.cn/SYSTEMS/Officialdocument/201912/P020200323536112807882.atx

CSNO (2019b) Satellite information of BDS. China Satellite Navigation Office, http://en.beidou.gov.cn/SYSTEMS/Officialdocument/201912/P020200323536298695483.zip

Dilssner F (2017) A note on the yaw attitude modeling of BeiDou IGSO-6. http://navigation-office.esa.int/attachments_24576369_1_BeiDou_IGSO-6_Yaw_Modeling.pdf

Dilssner F, Springer T, Flohrer C, Dow J (2010) Estimation of phase center corrections for GLONASS-M satellite antennas. J Geod 84(8):467–480. https://doi.org/10.1007/s00190-010-0381-7

Dilssner F, Springer T, Schönemann E, Enderle W (2014) Estimation of satellite antenna phase center corrections for BeiDou. In: Proceedings of IGS workshop 2014, June 23–27, Pasadena, USA

Dilssner F, Schönemann E, Mayer V, Springer T, Gonzalez F, Enderle W (2020) Recent advances in Galileo and BeiDou precise orbit determination at ESA's Navigation Support Office. EGU General Assembly 2020, Online, 4–8 May 2020, Vienna

Duan B, Hugentobler U, Selmke I (2019) The adjusted optical properties for Galileo/BeiDou-2/QZS-1 satellites and initial results on BeiDou-3e and QZS-2 satellites. Adv Space Res 63(5):1803–1812. https://doi.org/10.1016/j.asr.2018.11.007

Fliegel H, Gallini T, Swift E (1992) Global positioning system radiation force model for geodetic applications. J Geophys Res 97(B1):559–568. https://doi.org/10.1029/91JB02564

Folkner W, Williams J, Boggs D (2009) The planetary and lunar ephemeris DE 421. IPN Prog Rep 42–178. Jet Propulsion Laboratory

Ge M, Gendt G, Dick G, Zhang FP, Reigber C (2005a) Impact of GPS satellite antenna offsets on scale changes in global network solutions. Geophys Res Lett 32(6):L06310. https://doi.org/10.1029/2004GL022224

Ge M, Gendt G, Dick G, Zhang FP (2005b) Improving carrier-phase ambiguity resolution in global GPS network solutions. J Geod 79(1–3):103–110. https://doi.org/10.1007/s00190-005-0447-0

Guo J, Xu X, Zhao Q, Liu J (2016) Precise orbit determination for quad-constellation satellites at Wuhan University: strategy, result validation, and comparison. J Geod 90(2):143–159. https://doi.org/10.1007/s00190-015-0862-9

Guo J, Wang C, Chen G, Xu X, Zhao Q (2023) BDS-3 precise orbit and clock solution at Wuhan University: status and improvement. J Geod 97(2):15. https://doi.org/10.1007/s00190-023-01705-5

Huang G, Yan X, Zhang Q, Liu C, Wang L, Qin Z (2018) Estimation of antenna phase center offset for BDS IGSO and MEO satellites. GPS Solut 22(2):49. https://doi.org/10.1007/s10291-018-0716-z

Johnston G, Riddell A, Hausler G (2017) The International GNSS Service. In: Teunissen PJG, Montenbruck O (eds), Springer handbook of global navigation satellite systems. Springer International Publishing. pp 967–982. https://doi.org/10.1007/978-3-319-42928-1_33

Li X, Hu X, Guo R, Tang C, Zhou S, Liu S, Chen J (2018) Orbit and positioning accuracy for new generation BeiDou satellites during the Earth eclipsing period. J Navig 71(5):1069–1087. https://doi.org/10.1017/S0373463318000103

Li X, Yuan Y, Huang J, Zhu Y, Wu J, Xiong Y, Li X, Zhang K (2019) Galileo and QZSS precise orbit and clock determination using new satellite metadata. J Geod 93(8):1123–1136. https://doi.org/10.1007/s00190-019-01230-4

Li X, Yuan Y, Zhu Y, Jiao W, Bian L, Li X, Zhang K (2020) Improving BDS-3 precise orbit determination for medium earth orbit satellites. GPS Solut 24(2):53. https://doi.org/10.1007/s10291-020-0967-3

Li X, Han X, Li X, Liu G, Feng G, Wang B, Zheng H (2021) GREAT-UPD: An open-source software for uncalibrated phase delay estimation based on multi-GNSS and multi-frequency observations. GPS Solut 25(2):66. https://doi.org/10.1007/s10291-020-01070-2

Masoumi S (2022) Extension of the trial period for the switch to IGS20/igs20.atx and repro3 standards. IGSMAIL-8256. https://lists.igs.org/pipermail/igsmail/2022/008252.html

Pavlis N, Holmes S, Kenyon S, Factor J (2012) The development and evaluation of the Earth Gravitational Model 2008 (EGM2008). J Geophys Res Solid Earth 117(B04406). https://doi.org/10.1029/2011JB008916

Petit G, Luzum B (2010) IERS Conventions 2010. No.36 in IERS Technical Note, Verlag des Bundesamtes für Kartographie und Geodäsie, Frankfurt am Main, Germany

Qu Z, Guo J, Zhao Q (2021) Phase center corrections for BDS IGSO and MEO satellites in IGb14 and IGSR3 frame. Remote Sens 13(4):745. https://doi.org/10.3390/rs13040745

Rebischung P, Schmid R (2016) IGS14/igs14.atx: a new framework for the IGS products. In: Proceedings of AGU 2016 Fall Meeting, December 12–16, San Francisco, CA, USA

Rebischung P, Griffiths J, Ray J, Schmid R, Collilieux X, Garayt B (2012) IGS08: the IGS realization of ITRF2008. GPS Solut 16(4):483–494. https://doi.org/10.1007/s10291-011-0248-2

Rodriguez-Solano CJ, Hugentobler U, Steigenberger P, Lutz S (2011) Impact of Earth radiation pressure on GPS position estimates. J Geod 86(5):309–317. https://doi.org/10.1007/s00190-011-0517-4

Rodriguez-Solano C, Hugentobler U, Steigenberger P (2012) Adjustable box-wing model for solar radiation pressure impacting GPS satellites. Adv Space Res 49(7):1113–1128. https://doi.org/10.1016/j.asr.2012.01.016

Schmid R, Steigenberger P, Gendt G, Ge M, Rothacher M (2007) Generation of a consistent absolute phase-center correction model for GPS receiver and satellite antennas. J Geod 81(12):781–798. https://doi.org/10.1007/s00190-007-0148-y

Schmid R, Dach R, Collilieux X, Jäggi A, Schmitz M, Dilssner F (2016) Absolute IGS antenna phase center model igs08.atx: status and potential improvements. J Geod 90(4):343–364. https://doi.org/10.1007/s00190-015-0876-3

Schmitz M, Wübbena G, Propp M (2008) Absolute robot-based GNSS antenna calibration—features and findings. In: Proceedings of Internat Symposium on GNSS. Space-based and ground-based augmentation systems and applications, Berlin, Germany, pp 52–54

Steigenberger P, Thoelert S, Montenbruck O (2017) GNSS satellite transmit power and its impact on orbit determination. J Geod 92(6):609–624. https://doi.org/10.1007/s00190-017-1082-2

Villiger A (2022) Upcoming switch to IGS20/igs20.atx and repro3 standards. IGSMAIL-8238. https://lists.igs.org/pipermail/igsmail/2022/008234.html

Wanninger L, Beer S (2015) BeiDou satellite-induced code pseudorange variations: diagnosis and therapy. GPS Solut 19(4):639–648. https://doi.org/10.1007/s10291-014-0423-3

Xia F, Ye S, Chen D, Wu J, Wang C, Sun W (2020) Estimation of antenna phase center offsets for BeiDou IGSO and MEO satellites. GPS Solut 24(4):90. https://doi.org/10.1007/s10291-020-01002-0

Zajdel R, Steigenberger P, Montenbruck O (2022) On the potential contribution of BeiDou-3 to the realization of the terrestrial reference frame scale. GPS Solut 26(4):109. https://doi.org/10.1007/s10291-022-01298-0

Zhao Q, Guo J, Wang C, Lyu Y, Xu X, Yang C, Li J (2022) Precise orbit determination for BDS satellites. Satellite Navigation 3:2. https://doi.org/10.1186/s43020-021-00062-y

Yongqiang Yuan is a postdoc at the School of Geodesy and Geomatics at Wuhan University. He received his Ph.D. degree at the School of Geodesy and Geomatics at Wuhan University in 2022. His research area currently focuses on precise orbit determination and geodetic parameter estimation.

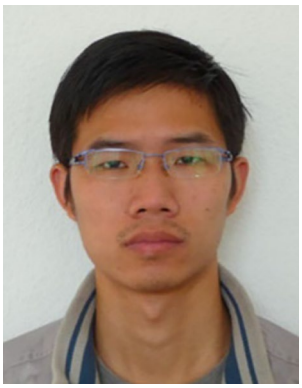

Xingxing Li is a professor at Wuhan University. He received his B.Sc. degree at the School of Geodesy and Geomatics, Wuhan University and obtained his Ph.D. degree at the Department of Geodesy and Remote Sensing, German Research Center for Geosciences (GFZ). His current research mainly involves satellite navigation and multi-sensor fusion.

Yibin Yao is a professor at the School of Geodesy and Geomatics at Wuhan University. He received his Ph.D. degree in Geodesy and Surveying Engineering from Wuhan University in 2004. His current research interest is in the GNSS ionospheric, atmospheric, and meteorological studies and high-precision GNSS data processing.

Shi Huang completed his B.Sc. degree in Surveying and Mapping Engineering at Wuhan University in 2020. Currently, he is a Master's student at the School of Geodesy and Geomatics at Wuhan University, and his research area mainly focuses on precise orbit determination for GNSS and LEO satellites.

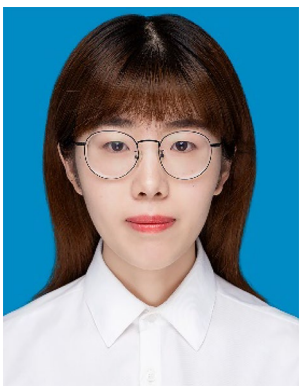

Qingyun Wang has completed her B.Sc. degree in Surveying and Mapping Engineering at Wuhan University in 2020. She is currently a Master's student at the School of Geodesy and Geomatics at Wuhan University, and she mainly focuses on the research of high-precision GNSS data processing and real-time positioning, navigation, and timing technologies.

Keke Zhang is a postdoc at the School of Geodesy and Geomatics at Wuhan University. He has completed his Ph.D. degree at the School of Geodesy and Geomatics, Wuhan University, in 2022. His research currently focuses on LEO precise orbit determination and LEO-augmented navigation technologies.